Anal. Chem. **2001,** *73,* 1979−1986

Analytical Solution of Combined Electroosmotic/Pressure Driven Flows in Two-Dimensional Straight Channels: Finite Debye Layer Effects

Prashanta Dutta and Ali Beskok*

Microfluidics Laboratory, Mechanical Engineering Department, Texas A&M University, College Station, Texas 77843-3123

Analytical results for the velocity distribution, mass flow rate, pressure gradient, wall shear stress, and vorticity in mixed electroosmotic/pressure driven flows are presented for two-dimensional straight channel geometry. We particularly analyze the electric double-layer (EDL) region near the walls and define three new concepts based on the electroosmotic potential distribution. These are the effective EDL thickness, the EDL displacement thickness, and the EDL vorticity thickness. We show that imposing Helmholtz−Smoluchowski velocity at the edge of the EDL as the velocity matching condition between the EDL and the bulk flow region is incomplete under spatial bulk flow variations across the finite EDL. However, the Helmholtz−Smoluchowski velocity can be used as the appropriate slip velocity on the wall. We discuss the limitations of this approach in satisfying the global conservation laws.

Recent developments in microfabrication technologies have enabled a variety of miniaturized fluidic systems, which can be utilized for medical, pharmaceutical, defense, and environmental monitoring applications. Examples of such applications are drug delivery,[1] DNA analysis/sequencing systems,[2] and biological/chemical agent detection sensors on microchips. Along with the necessary sensors and electronic units, these devices include various fluid handling components such as microchannels, pumps,[3] and valves. Utilization of electrokinetic body forces in microfluidic design can revolutionize various fluid handling applications, since it will be possible to build flow control elements with *nonmoving components*.

The electrokinetic effects were first discovered by Reuss[4] in 1809 from an experimental investigation on porous clay, which was followed by experiments of Wiedmann.[5] In 1879, Helmholtz developed the electric double-layer (EDL) theory, relating the electric and flow parameters for electrokinetic transport. The case of EDL thickness being much smaller than the channel dimensions was analyzed by von Smoluchowski, who also derived a velocity *slip condition* for electroosmotically driven flows.[6] Electroosmotic flows in thin two-dimensional slits and thin cylindrical capillaries were analyzed by Burgreen and Nakache[7] and Rice and Whitehead,[8] respectively. In 1952, Overbeek proposed the irrotationality condition of internal electrosomotic flows for arbitrarily shaped geometry.[9] This was followed by the *ideal electroosmosis concept* of Cummings et al., who showed similarity between the electric and the velocity fields under some specific outer field boundary conditions.[10,11] In the past decade, there have been numerous theoretical,[12,13] numerical,[14−17] and experimental[18,19] studies on electrokinetic microflows.

Microchannels are one of the primary components of microfluidic systems. Motivated by the development of fluid handling devices with nonmoving components, in this paper, we study the combined electroosmotic/pressure driven flows in straight two-dimensional channels. Our analysis is particularly important for *small, yet finite electric double-layer* applications, where the distance between the two walls of a microfluidic device is about 1−3 orders of magnitude larger than the electric double layer. This is commonly observed in channel dimensions of 10 μm or less, depending on the ionic concentration. Currently, it is possible to build microchannels with 1 μm or smaller dimensions. For example, Chen et al.[20] recently built an electrokinetic pump with dimensions of 40 mm × 1 mm × 1 μm. Although it may be very difficult to perform pointwise measurements in micrometer and

* Corresponding author: (e-mail) abeskok@mengr.tamu.edu; (phone) (979) 862 1073.

(1) Arangoa, M. A.; Campanero, M. A.; Popineau, Y.; Irache, J. M. *Chromatographia* **1999**, *50* (3−4), 243−246.
(2) Chang, H. T.; Chen, H. S.; Hsieh, M. M.; Tseng, W. L. *Rev. Anal. Chem.* **2000**, *19* (1), 45−74.
(3) DeCourtye, D.; Sen, M.; Gad-El-Hak M. *Int J. Comput. Fluid Dyn.* **1998**, *10* (1) 13−25.
(4) Reuss, F. F. *Memoires de la Societe Imperiale de Naturalistes de Moscou* **1809**, *2*, 327.
(5) Wiedemann, G. *Pogg. Ann.* **1852**, *87*, 321.
(6) Smoluchowski, M. *Krak. Anz.* **1903**, 182.
(7) Burgreen, D.; Nakache, F. R. *J. Phys. Chem.* **1964**, *68*, 1084−1091.
(8) Rice, C. L.; Whitehead, R. J. *J. Phys. Chem.* **1965**, *69*, 4017−4023.
(9) Overbeek, J. T. G. In *Colloid Science;* Kruyt, H. R., Ed.; Elsevier Publishing Co.: Amsterdam, 1952; Vol. 1.
(10) Cummings, E. B.; Griffiths, S. K.; Nilson, R. H. *Proc. SPIE Microfluidic Devices Syst. II* **1999**, *3877*, 180−189.
(11) Cummings, E. B.; Griffiths, S. K.; Nilson, R. H.; Paul, P. H. *Anal. Chem.* **2000**, *72*, 2526−2532.
(12) Ohshima, H.; Kondo, T. *J. Colloid Interface Sci.* **1990**, *135* (2), 443−448.
(13) Keh, H. J.; Liu, Y. C. *J. Colloids Interface Surf.* **1995**, *172*, 222−229.
(14) Ermakov, S. V.; Jacobson, S. C.; Ramsey, J. M. *Anal. Chem.* **1998**, *70*, 4494−4504.
(15) Patankar, N. A.; Hu, H. H. *Anal. Chem.* **1998**, *70*, 1870−1881.
(16) Yang, C.; Li, D.; Masliyah, J. H. *Int. J. Heat Mass Transfer* **1998**, *41*, 4229−4249.
(17) Bianchi, F.; Ferrigno, R.; Girault, H. H. *Anal. Chem.* **2000**, *72*, 1987−1993.
(18) Jacobson, S. C.; McKnight, T. E.; Ramsey, J. M. *Anal. Chem.* **1999**, *71*, 4455−4459.
(19) Culbertson, C. T.; Ramsey, R. S.; Ramsey, J. M. *Anal. Chem.* **2000**, *72*, 2285−2291.
(20) Chen, C. H.; Zeng, S.; Mikkelsen, J. C.; Santiago, J. G. *Proc. ASME* **2000**, *MEMS 1*, 523−528.

10.1021/ac001182i CCC: $20.00
Published on Web 03/22/2001

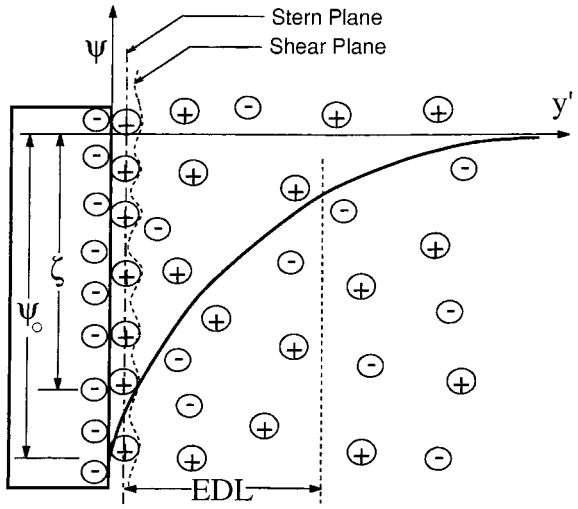

Figure 1. Schematic diagram of the electric double layer (EDL) next to a negatively charged solid surface. Here ψ is the electric potential, ψ_o is the surface electric potential, ζ is the zeta potential, and y' is the distance measured from the wall.

submicrometer scales, the drive for further miniaturization requires study of finite Debye layer effects.

This paper is organized as follows: We first present an analytic solution for the electroosmotic potential distribution and describe an effective EDL thickness by concentrating on the near-wall region. We then present the governing equations for fluid flow and obtain analytic solutions for the fluid velocity, pressure, and shear stress from the streamwise momentum equation. This is followed by a discussion of the limitations of the appropriate velocity slip boundary conditions for simplified engineering analysis. Finally, we present our conclusions.

ELECTRIC DOUBLE LAYER

The electric double layer is formed due to the interaction of ionized solution with static charges on dielectric surfaces.[21] For example, a glass surface immersed in water undergoes a chemical reaction in which a fraction of the surface silanol group SiOH are changed to SiO^- or $SiOH_2^+$, resulting in a net negative or positive surface potential depending on P^H of the electrolyte. This influences distribution of the ions in the buffer solution, as shown in Figure 1. The ions of opposite charge cluster immediately near the wall forming the *Stern layer*, a layer of typical thickness of one ionic diameter. The ions within the Stern layer are attracted to the wall with very strong electrostatic forces, as recently shown by molecular dynamics studies.[22] Immediately after the Stern layer there forms the electric double layer, where the ion density variation obeys the Boltzmann distribution, consistent with the derivation based on statistical mechanical considerations.[23] For a symmetric electrolyte, the electric potential distribution due to the presence of the EDL is described by the Poisson−Boltzmann equation[21]

$$\nabla^2(\psi^*) = \frac{-4\pi h^2 \rho_e}{D\zeta} = \beta \sinh(\alpha\psi^*) \qquad (1)$$

where the ψ^* ($= \psi/\zeta$) is the electroosmotic potential normalized with the zeta potential ζ, ρ_e is the net electric charge density, D is the dielectric constant, and α is the ionic energy parameter given as

$$\alpha = ez\zeta/k_bT \qquad (2)$$

where e is the electron charge, z is the valence, k_b is the Boltzmann constant, and T is the temperature. The variable β relates the ionic energy parameter α and the characteristic length h to the Debye−Hückel parameter ω as

$$\beta = (\omega h)^2/\alpha \qquad (3)$$

where

$$\omega = \frac{1}{\lambda} = \sqrt{\frac{8\pi n_o e^2 z^2}{Dk_bT}} \qquad (4)$$

The Debye length (λ) is a function of the ion density n_o as given by eq 4. For aqueous solutions at 25 °C, the ion densities of 1 and 100 mol/m^3 correspond to the Debye lengths of $\lambda = 10$ nm, and $\lambda = 1$ nm, respectively.

For our analysis, we consider a two-dimensional channel as shown in Figure 2. We assume that the zeta potential ζ is known, and it remains constant along the channel. Under these conditions, eq 1 is simplified in the following form:

$$\frac{d^2\psi^*}{d\eta^2} = \beta \sinh(\alpha\psi^*) \qquad (5)$$

where $\eta = y/h$ and h is the half channel height. Multiplying both sides of this equation by $2(d\psi^*/d\eta)$, and integrating with respect to η, the following relation is obtained:[7]

$$\frac{d\psi^*(\eta)}{d\eta} = \sqrt{\frac{\beta}{\alpha}}[2\cosh(\alpha\psi^*) - 2\cosh(\alpha\psi_c^*)]^{1/2} \qquad (6)$$

where both the electric potential and its spatial gradient at point η are represented as a function of the electric potential at the channel center (i.e., $\psi_c^* = \psi_{\eta=0}^*$).

An analytical solution of eq 5 was obtained by Burgreen and Nakache[7] in terms of a first-kind elliptic integral for finite EDL thickness, where the two channel walls may interact with each other. Their work presents the potential distribution as a function of the Debye length λ and the ionic energy parameter α. In ref 24, we have shown with extensive numerical simulations that for $\alpha \geq 1$ and $\lambda \ll h$ the electric potential in the middle of the channel is practically zero. When $\psi_c^* = 0$, the last term in eq 6 is simplified. Hence, using the identity $\cosh(p) = 2\sinh^2(p/2) + 1$, eq 6 can be integrated once more. This results in the following

(21) Probstein, R. F. *Physiochemical Hydrodynamics: An Introduction;* Wiley and Sons: New York, 1994.
(22) Lyklema, J.; Rovillard, S.; Coninck, J. D. *J. Surf. Colloids* **1994**, *14* (20), 5659−5663.
(23) Feynman, R. P.; Leighton, R. B.; Sands, M. *The Feynman Lectures on Physics;* Addison-Wesley: Reading, MA, 1977.
(24) Dutta, P.; Warburton, T. C.; Beskok, A. *Proc. ASME* **1999**, *MEMS 1*, 467−474.

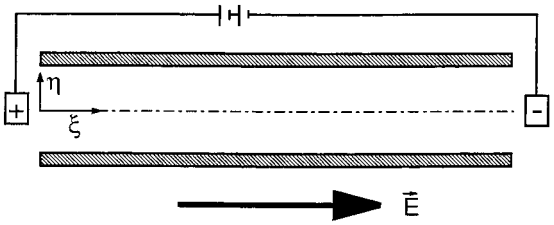

Figure 2. Schematic view of the elecroosmotic flow between two parallel plates. The external electric field is indicated by $\vec{E}$.

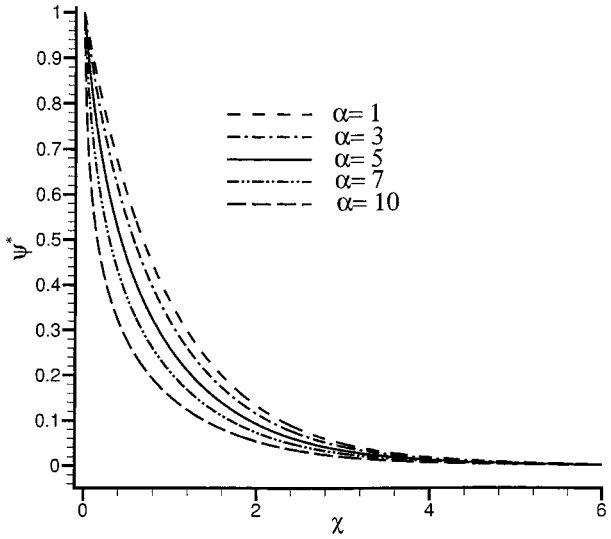

Figure 3. Electrosmotic potential distribution within the electric double layer as a function of the inner-layer scale $\chi = \omega y'$.

form, as shown earlier by Hunter:[25]

$$\psi^*(\eta^*) = \frac{4}{\alpha}\tanh^{-1}\left[\tanh\left(\frac{\alpha}{4}\right)\exp(-\sqrt{\alpha\beta}\eta^*)\right] \qquad (7)$$

where η^* is the normalized distance from the wall (i.e., $\eta^* = 1 - |\eta|$).

NEAR-WALL POTENTIAL DISTRIBUTION

In this section, we present the potential distribution as a function of the near-wall parameter $\chi = y'\omega$, where $y' = h - y$ is the distance from the wall and ω is the Debye−Hückel parameter given by eq 4. Since $\omega h = (\alpha\beta)^{1/2}$, the near-wall scaling parameter (χ) and the nondimensional distance from the wall (η^*) can be represented in terms of each other (i.e., $\chi = (\alpha\beta)^{1/2}\eta^*$). On the basis of this, eq 7 can be simplified as

$$\psi^* = \frac{4}{\alpha}\tanh^{-1}\left[\tanh\left(\frac{\alpha}{4}\right)\exp(-\chi)\right] \qquad (8)$$

It is clear that the *inner layer scaling* of the potential distribution is independent of β for $\lambda \ll h$. In Figure 3 we present the near-wall potential distribution ψ^* as a function of χ for several α values. We observe that the electroosmotic potential decays to zero with increased χ for all these cases. We quantify this decay by presenting a logarithmic plot of the electroosmotic potential in the near-wall region as a function of χ in Figure 4. A careful examination of Figure 4 shows *exponential decay* of the electroosmotic potential with slope −1 for $\chi > 2$. This result can be easily verified by expanding eq 8 for $\chi > 2$, where $\tanh(\alpha/4) \leq 1$, and $\exp(-\chi) \ll 1$. Under these conditions

$$\psi^*(\chi) \simeq \frac{4}{\alpha}\tanh\left(\frac{\alpha}{4}\right)\exp(-\chi) \qquad (9)$$

which was also shown earlier by Hunter.[25]

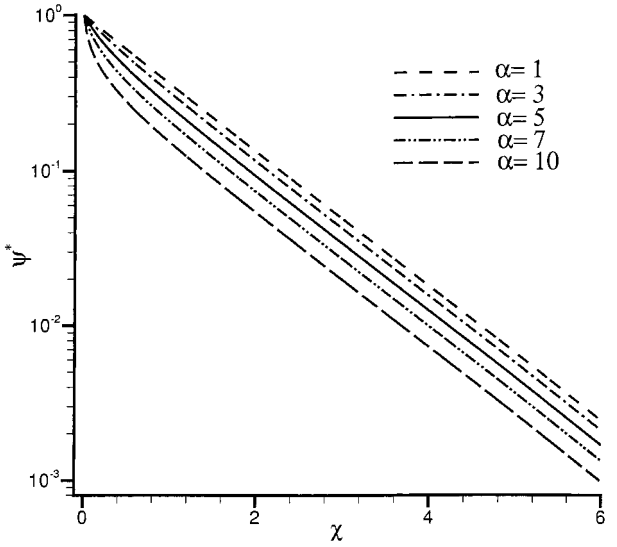

Figure 4. Logarithmic scaling of ψ^* variation as a function of the inner-layer scale χ.

GOVERNING EQUATIONS FOR FLUID FLOW

The electroosmotic flow is generated when an external electric field ($\vec{E} = -\nabla\phi$) is applied in the presence of the EDL. This external electric field interacts with the electric double layer and creates the electrokinetic body force on the bulk fluid. The motion of ionized, incompressible fluid with electroosmotic body forces is governed by the incompressible Navier−Stokes equations:

$$\rho_f\left(\frac{\partial\vec{V}}{\partial t} + (\vec{V}\cdot\nabla)\vec{V}\right) = -\nabla P + \mu\nabla^2\vec{V} + \rho_e\vec{E} \qquad (10)$$

where P is the pressure, $\vec{V} = (u, v)$ is a divergence free velocity field ($\nabla\cdot\vec{V} = 0$) subject to no-slip boundary conditions on the walls, and ρ_f is the fluid density. Here ρ_e is determined from eq 1. The externally imposed electric potential (ϕ) is governed by

$$\nabla\cdot(\sigma\nabla\phi) = 0 \qquad (11)$$

where σ is the conductivity and the electric potential is subject to the insulating boundary conditions ($\nabla\phi\cdot\vec{n} = 0$) on the walls. The ζ is assumed to be uniform on all surfaces, and Newtonian fluid with uniform properties is assumed throughout the flow.

ANALYSIS FOR CHANNEL FLOWS

In this section, we analyze the mixed electroosmotic/pressure driven flows in straight microchannels. We assume that the channel height h is much smaller than the channel width W (i.e.,

(25) Hunter, R. J. *Zeta Potential in Colloid Science: Principles and Applications*; Academic Press: New York, 1981.

$h \ll W$). Hence, the flow can be treated as two-dimensional as shown in Figure 2. We also assume fully developed, steady flow with no-slip boundary conditions.

The streamwise momentum equation is given by

$$\frac{\partial P}{\partial x} = \mu \frac{\partial^2 u}{\partial y^2} + \rho_e E_x \tag{12}$$

where u is the streamwise velocity and $E_x = -\mathrm{d}\phi/\mathrm{d}x$. Using eq 1 for ρ_e, we obtain

$$\frac{\partial P}{\partial x} = \mu \frac{\partial^2 u}{\partial y^2} - \frac{DE_x}{4\pi} \frac{\mathrm{d}^2 \psi}{\mathrm{d}y^2} \tag{13}$$

This equation is "linear", and hence we can decompose the velocity field into two parts:

$$u = u_{\mathrm{Pois}} + u_{\mathrm{elec}}$$

where u_{Pois} corresponds to the pressure driven channel flow velocity (i.e., plane Poiseuille flow) and u_{elec} is the electroosmotic flow velocity. Analysis of eq 13 in the absence of the pressure gradients results in balance between the viscous diffusion terms and the electroosmotic forces, which leads to the Helmholtz−Smoluchowski electroosmotic velocity u_{HS}:[21]

$$u_{\mathrm{HS}} = -ME_x = -\zeta DE_x/4\pi\mu = -\frac{\zeta \epsilon E_x}{\mu} \tag{14}$$

where M is the mobility ($M = \zeta D/4\pi\mu$).

We nondimensionalize eq 13 and present the nondimensional streamwise momentum equation:

$$\frac{\partial P^*}{\partial \xi} = \frac{\partial^2 U}{\partial \eta^2} + \frac{\mathrm{d}^2 \psi^*}{\mathrm{d}\eta^2} \tag{15}$$

where $U = u/u_{\mathrm{HS}}$, $P^* = P/(\mu u_{\mathrm{HS}}/h)$, and $\xi = x/h$. Here pressure is normalized by the viscous forces, rather than the dynamic head, consistent with the Stokes flow formulation.

In the case of zero net pressure gradient, one can easily integrate eq 15 to obtain,

$$U(\eta) = 1 - \psi^*(\eta) \tag{16}$$

which was shown earlier by Burgreen and Nakache.[7]

In the limit of small, yet finite Debye layers the electroosmotic potential ψ^* decays very fast within the thin electric double layer and a uniform "pluglike" velocity profile is obtained in most of the channel. The plug flow behavior has been observed in various experiments.[26−28]

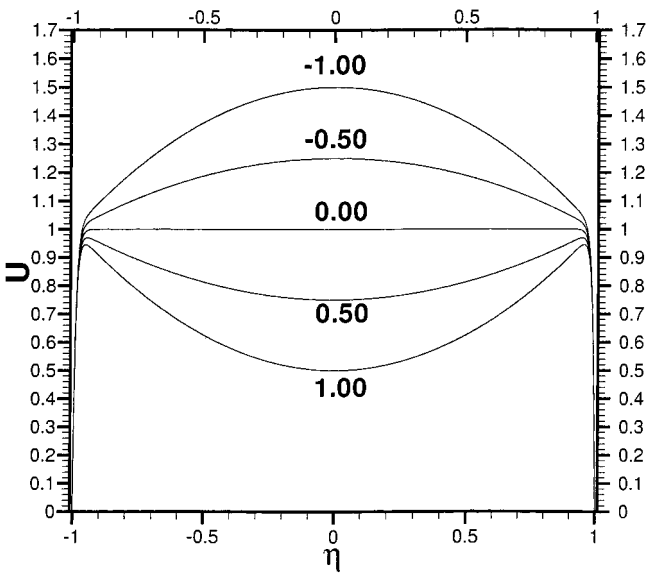

Figure 5. Velocity distribution in mixed electroosmotic/pressure driven flows under various values of the streamwise pressure gradient $\mathrm{d}P^*/\mathrm{d}\xi$. The $\mathrm{d}P^*/\mathrm{d}\xi = 0$ corresponds to a "pluglike flow". The results are plotted for $\alpha = 1$ and $\beta = 10\,000$ using eq 17.

For the mixed electroosmotic/pressure driven flows, we use the superposition principle for linear equations and obtain the following nondimensional velocity profile.

$$U(\eta) = -\frac{1}{2}\frac{\mathrm{d}P^*}{\mathrm{d}\xi}(1 - \eta^2) + 1 - \psi^*(\eta) \tag{17}$$

where $\mathrm{d}P^*/\mathrm{d}\xi$ corresponds to the pressure gradient in the mixed electroosmotic/pressure driven flow regime. We can substitute the solution for ψ^* from eq 7 to obtain an analytical formula for the velocity distribution. In Figure 5 we show velocity profiles for various pressure gradients. The case for $\mathrm{d}P^*/\mathrm{d}\xi = 0$ corresponds to a pure "pluglike flow", and the cases $\mathrm{d}P^*/\mathrm{d}\xi < 0$ and $\mathrm{d}P^*/\mathrm{d}\xi > 0$ correspond to flows with favorable and adverse pressure gradients, respectively.

The velocity profiles shown in Figure 5 correspond to $\alpha = 1$ and $\beta = 10\,000$. This is an example of 0.1 mM aqueous solution in glass channel with ζ of 25.4 mV. The Debye length estimated by eq 4 is 30 nm, and hence, the channel height is ~6.0 μm. Alternatively, for 1 mM concentration, the Debye length becomes 10 nm, which corresponds to a 2-μm channel height. In the dimensional examples given above, as well as from the normalized solution shown in Figure 5, it is apparent that the *Debye layer effects in such small dimensions are finite.* Hence, the presence of the EDL cannot be totally neglected. For example, the velocity distribution within the EDL will result in a flow rate defect, if the bulk flow is assumed to extend up to the wall. This flow rate defect is analogous to the *boundary layer displacement thickness* in fluid mechanics.

To obtain the mass flow rate, we must integrate the velocity and, hence, the electroosmotic potential distribution across the channel (See eq 17). This can be cumbersome in the η-coordinate system, where ψ^* is a function of both α and β. However, in the χ-coordinate system, ψ^* is only a function of α. Hence, we define the *electric double-layer displacement thickness* δ^* in analogy to the

(26) Molho, J. M.; Herr, A. E.; Desphande, M.; Gilbert, J. R.; Garguilo, M. G.; Paul, P. H.; John, P. M.; Woudenberg, T. M.; Connel, C. *Proc. ASME (MEMS)* **1998**, *66*, 69−76.
(27) Paul, P. H.; Garguilo, M. G.; Rakestraw, D. J. *Anal. Chem.* **1998**, *70*, 2459−2467.
(28) Herr, A. E.; Molho, J. I.; Santiago, J. G.; Mungal, M. G.; Kenny, T. W.; Garguilo, M. G. *Anal. Chem.* **2000**, *72*, 1053−1057.

Table 1. Variation of the EDL Displacement Thickness δ^*, the Effective EDL Thickness δ_{99}, and the EDL Vorticity Thickness Ω_{99} as a Function of the Ionic Energy Parameter α[a]

	α				
	1	3	5	7	10
δ^*	0.98635	0.89156	0.75670	0.62702	0.47731
δ_{99}	4.5846	4.4390	4.2175	3.9852	3.6756
Ω_{99}	4.5846	4.439	4.2176	3.9854	3.6760

[a] The values of δ^*, δ_{99}, and Ω_{99} are given in terms of the Debye length λ.

boundary layer displacement thickness in fluid mechanics in the following form:

$$\delta^* = \int_0^{\hat{\chi}} \psi^* \, d\chi \tag{18}$$

where $\hat{\chi}$ is a large enough distance that includes variations of ψ^* as observed from Figure 3. For example, $\hat{\chi} \simeq 10$ is sufficient to accurately define the δ^*. Typical values of δ^* as a function of α are presented in Table 1. The physical meaning of δ^* is the volumetric flow rate defect due to the velocity distribution within the EDL.

Integration of the ψ^* term in eq 17 is performed by using eq 18, where

$$\int_{-1}^{1} \psi^* \, d\eta = 2\int_0^1 \psi^* \, d\eta = \frac{2}{\sqrt{\alpha\beta}} \int_0^{\hat{\chi}} \psi^* \, d\chi = \frac{2\delta^*}{\sqrt{\alpha\beta}}$$

The resulting volumetric flow rate per channel width, normalized by $u_{HS}h$ becomes

$$\dot{Q} = -\frac{2}{3}\frac{dP^*}{d\xi} + 2\left(1 - \frac{\delta^*}{\sqrt{\alpha\beta}}\right) \tag{19}$$

Since most of the microfluidic experiments are performed by imposing a certain amount of pressure drop along the microchannel, one can use eq 19 to correlate the volumetric flow rate with the imposed pressure drop. Also, for applications with specified volumetric flow rate, one can obtain the resulting pressure variation along the channel.

We find the shear stress on the wall for the mixed pressure/electroosmotically driven flow region by differentiating eq 17 with respect to η and utilizing eq 6. This results in

$$\tau_w^* = \sqrt{\frac{\beta}{\alpha}}\sqrt{2\cosh(\alpha) - 2\cosh(\alpha\psi_c)} - \frac{dP^*}{d\xi} \tag{20}$$

where the shear stress is normalized with $\mu u_{HS}/h$. This is an implicit *exact* relation under the assumptions of our analysis, which require ψ_c^*. Assuming that $\psi_c^* = 0$ (valid for $\alpha \geq 1$ and $\lambda \ll h$), we find an approximate relation for the normalized shear stress:

$$\tau_w^* = \sqrt{\frac{\beta}{\alpha}}\sqrt{2\cosh(\alpha) - 2} - \frac{dP^*}{d\xi} \tag{21}$$

The first term on the right-hand side is due to the variation of velocity within the EDL, and the second term is due to the parabolic velocity profile of the bulk flow.

For infinitesimally small EDL, Overbeek[9] and Cummings et al.[11] have independently shown the similarity between the externally applied electric field and the *bulk flow field*, under certain conditions. According to this similarity, the bulk flow is a potential flow. Since the potential flows are irrotational, the bulk flow vorticity is zero. The vorticity ($\Omega = \nabla \times \vec{V}$) shows fluid rotation, and it is twice the local angular velocity. In "pure electroosmotic flows", the matching condition between the bulk flow region and the EDL region is usually modeled by the Helmholtz−Smoluchowski electroosmotic velocity (eq 14).

For finite EDL, we would like to quantify the penetration of EDL vorticity to the bulk flow region. This is important to characterize the interface and the matching conditions between the EDL and the bulk flow region. A relationship for fluid vorticity can be obtained by differentiating U with respect to η, since the cross-flow velocity component $V = 0$, everywhere in the channel

$$\Omega = -\frac{dU}{d\eta} = -\frac{dP^*}{d\xi}\eta + \frac{d\psi^*}{d\eta} \tag{22}$$

Vorticity due to the pressure driven flow, given by the first term, is trivial. However, the vorticity component due to the electroosmotic "plug flow" is present within the EDL, and its value needs to be quantified. For this purpose, we concentrate only on the electroosmotic vorticity (assuming $dP^*/d\xi = 0$) and utilize eq 6 in the χ-coordinate system

$$\frac{d\psi^*}{d\chi} = \left(\frac{1}{\alpha}\right)[2\cosh(\alpha\psi^*) - 2]^{1/2} \tag{23}$$

Using the identity $\cosh(p) = 2\sinh^2(p/2) + 1$, we simplify the above equation as

$$\frac{d\psi^*}{d\chi} = \frac{2}{\alpha}\sinh\left(\frac{\alpha\psi^*}{2}\right) \tag{24}$$

The variation of $d\psi^*/d\chi$ as a function of χ is shown in Figure 6 for various α values. Exponential decay of the electroosmotic flow vorticity with slope of -1 is observed for $\chi > 2$. This can be verified analytically. Since for $\chi \geq 2$, $\psi^* \ll 1$, and $\sinh(\alpha\psi^*/2) \simeq \alpha\psi^*/2$. Hence, we get

$$\frac{d\psi^*}{d\chi} \simeq \psi^* \tag{25}$$

This is a very interesting result, as both the electroosmotic potential and its derivative decays exponentially for $\chi \geq 2$. A close observation of Figure 6 for $\chi < 0.5$ shows that the rate of decay of $d\psi^*/d\chi$ is *faster than exponential* for $\alpha > 1$.

Besides the EDL displacement thickness δ^*, we define two additional parameters, in analogy to the boundary layer theory. The first one is the *effective EDL thickness* (δ_{99}), defined as the distance from the wall in terms of λ, where the electroosmotic potential decays to 1% of its original value. For pure electroosmotic flows, the velocity reaches 99% of its pure plug flow value at this

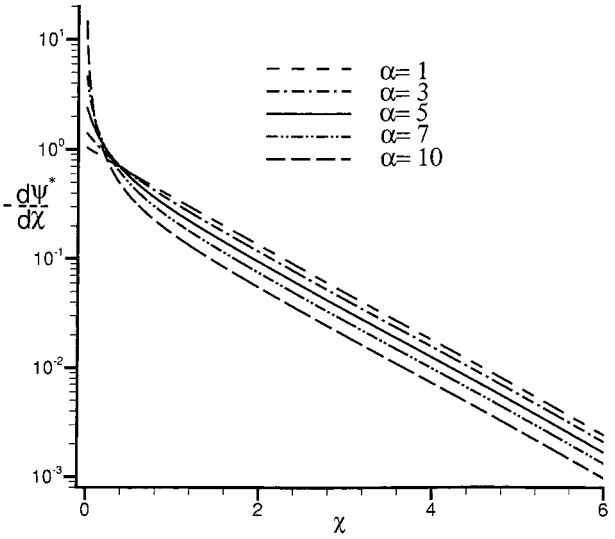

Figure 6. Variation of $d\psi^*/d\chi$ as a function of the inner-layer scale χ for various α values. This also corresponds to the vorticity variation within the electric double layer for "pure electroosmotic" flows.

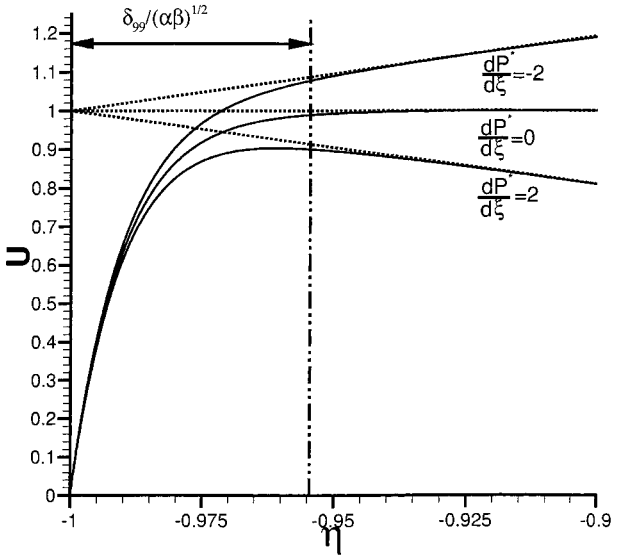

Figure 7. Magnified view of the velocity distribution in a mixed electroosmotic/pressure driven flow near a wall for $\alpha = 1$ and $\beta = 10\,000$. Extrapolation of the velocity using a parabolic velocity profile with constant slip value U_{HS} on the wall are shown by the dashed lines. The analytical solution is shown by the solid lines. If one chooses to implement a matching condition at the edge of the EDL ($\delta_{99}\lambda$), the appropriate slip condition is given by eq 27.

point. Another implication of the effective EDL thickness is discussed in the EDL/Bulk Flow Interface Velocity Condition section. The values of δ_{99} are presented as a function of the ionic energy parameter α in Table 1. One can calculate the value of δ_{99} in terms of the η^* coordinates by dividing the value of δ_{99} given in Table 1 by $(\alpha\beta)^{1/2}$. Finally, the dimensional value of the effective EDL thickness can be found by multiplying δ_{99} with the Debye length (λ). For $\alpha = 1$ and $\beta = 10\,000$, using the earlier dimensional examples of 6-μm channel height with 0.1 mM concentration corresponds to $\delta_{99} = 137$ nm. Hence, δ_{99} is 4.5% of the channel half-height, a portion significantly large, yet too small to be resolved by the current experimental techniques.

We also define an *electric double-layer vorticity thickness* Ω_{99} as the distance from the wall (in terms of λ) when the nondimensional vorticity is reduced to $\Omega = 0.01$. Such a definition may become useful in identifying the boundary between the finite EDL and the bulk flow region, based on vorticity. Here, using the Ω_{99} concept, we define the distance from the wall, where the irrotationality condition can be (approximately) imposed. Typical values of Ω_{99} as a function of α are given in Table 1 in terms of λ. Comparing the values of Ω_{99} and δ_{99} in Table 1, we notice that these two quantities are approximately the same.

Since both the vorticity and the electroosmotic potential decay exponentially with χ (for $\chi \geq 2$), we could have used alternative cutoff distances (beyond 1% variation) in definition of the effective EDL and EDL vorticity thickness. Especially, the irrotational flow conditions will be satisfied better for smaller vorticity magnitudes than 1% of the EDL maximum vorticity. More restrictive definitions can be produced by using δ_{99} and Ω_{99} values given in Table 1 and adding $\log_e(10) \simeq 2.3$ to δ_{99} and Ω_{99} values for every additional 10-fold decrease. This is due to the exponential decay of both ψ^* and $d\psi^*/d\chi$ shown in Figures 4 and 6.

EDL/BULK FLOW INTERFACE VELOCITY CONDITION

In this section, we present the velocity matching condition between the EDL and the bulk flow regions for mixed electroosmotic/pressure driven flows. The interface velocity condition is important in order to assess the interaction of high-vorticity fluid in the EDL with vorticity of the bulk flow under various conditions. The commonly accepted interface matching condition described by the Helmholtz−Smoluchowski velocity (eq 14) will not be adequate to describe this interaction properly for small yet finite EDL thickness. A similar situation also exists in the regions of complex geometries, where the EDL thickness is comparable to the radius of curvature of the domain.

Our analysis assumes that the velocity near the surface can be decomposed into two components: one due to the electroosmotic effects, and the other due to the pressure driven bulk flow. Utilization of the Helmholtz−Smoluchowski velocity (eq 14) as the "matching condition" at one Debye length (λ) away from the wall is incomplete for the following two reasons. First, such a matching condition should be implemented at the *effective EDL thickness* ($\delta_{99}\lambda$), which is considerably larger than the Debye length predicted by the inverse Debye−Hückel parameter. The second limitation arises due to the variation of bulk velocity across the small yet finite EDL.

If we examine the velocity distribution at the edge of the EDL in Figure 7, it is clear that the matching velocity changes with the velocity gradient of the bulk flow region. Hence, the appropriate velocity matching condition (u_{match}) at the edge of the EDL ($y = \delta_{99}\lambda$) should become

$$u_{match} = \lambda\delta_{99}\frac{\partial u}{\partial y}\Big|_w + u_{HS} \qquad (26)$$

where $\partial u/\partial y|_w$ corresponds to the *bulk flow gradient obtained on the wall*. The appropriate matching distance is taken to be the effective EDL thickness ($\delta_{99}\lambda$). Equation 26 in normalized form becomes

$$U_{\text{match}} = \left(\frac{\delta_{99}}{\sqrt{\alpha\beta}}\right)\frac{\partial U}{\partial \eta}|_{\text{w}} + U_{\text{HS}} \qquad (27)$$

Here, the first term in eq 27 corresponds to a *Taylor series expansion* of bulk flow velocity at the edge of the EDL from the wall. Equation 27 is analogous to slip velocity in rarefied gas flows.[29] The analytical results in Figure 7 are for $\alpha = 1$ and $\beta = 10\,000$, which corresponds to 0.1 mM buffer solution in a 6-μm glass channel, with $\delta_{99} = 4.58\lambda = 0.137$ μm. It is noteworthy to mention that, for finite Debye layers with large bulk flow gradients, the velocity matching conditions using eq 27 will give *considerable deviations* from the Helmholtz−Smoluchowski prediction.

ELECTROOSMOTIC SLIP CONDITION

The electroosmotic forces are concentrated within the EDL, which has an effective thickness in the order of 100−1 nm. On the other hand, the microchannels utilized for many laboratory on a chip applications have a typical height of 100−1 μm. This 2−5 orders of magnitude difference in the EDL and the channel length scales is a great challenge in numerical simulation of electroosmotically driven microflows. Therefore, it is desired to develop a *unified slip condition*, which incorporates the EDL effects by specifying an appropriate velocity slip condition on the wall. Examining Figure 7 and eq 27, it is seen that the bulk velocity field extended onto the wall has a constant slip value equivalent to u_{HS}. Hence, the appropriate slip condition on the wall is the Helmholtz−Smoluchowski velocity u_{HS}, even for finite EDL thickness conditions.

For a general numerical algorithm, implementation of slip velocity u_{HS} on the walls *overpredicts* the volumetric flow rate, since the velocity distribution within the EDL is neglected. This flow rate error can be corrected by subtracting $2\delta^*/(\alpha\beta)^{1/2}$ (in nondimensional form) using the EDL displacement thickness δ^* given in Table 1. For engineering applications with $\alpha = 1$ and $\beta = 10\,000$, corresponding to 0.1 mM buffer solution in a 6-μm glass channel, the error in the conservation of mass equation due to this slip condition is ~4.5%.

In regard to the errors in the momentum equation, neglecting shear stresses due to the velocity distribution within the EDL, given by eq 21, will be in gross error. However for steady Stokes flows, the total drag force can be predicted using a control volume analysis and imposing Newton's second law within the entire control volume. This requires proper inclusion of the electrokinetic body forces. For example, the drag force can be predicted in numerical simulations at the *postprocessing stage*, by first solving the flow system with the slip condition and then calculating the over all drag by *approximating* the electroosmotic *body forces* concentrated on the *domain boundaries*.

Approximate Evaluation of Drag Force due to the Electrokinetic Effects. The drag force acting on a control volume due to the electrokinetic effects can be expressed as

$$\vec{F}_{\text{B}} = \int_{\text{CV}} \rho_{\text{e}} \vec{E}\, \text{d}V \qquad (28)$$

Substituting ρ_{e} from the Poisson−Boltzmann equation and $\vec{E} = -\nabla\phi$ we obtain

$$\vec{F}_{\text{B}} = \int_{\text{CV}} \epsilon \nabla^2 \psi \left[\frac{\partial \phi}{\partial n}\vec{e}_{\text{n}} + \frac{\partial \phi}{\partial l}\vec{e}_{\text{l}} + \frac{\partial \phi}{\partial s}\vec{e}_{\text{s}}\right] \text{d}V \qquad (29)$$

where n, l, and s are the normal, streamwise, and spanwise coordinates, respectively, and $\text{d}V = \text{d}n\ \text{d}s\ \text{d}l$. This volume integral is complicated to evaluate in general. However, some simplifications can be made when $\lambda/h \ll 1$. Also, for a general complex geometry, we further assume that the radius of curvature R is much larger than the Debye length λ. The latter condition is required to exclude application of the forthcoming procedure in the vicinity of sharp corners. On the basis of these assumptions, $\nabla^2\psi$ can be approximated to be $\text{d}^2\psi/\text{d}n^2$. Also, $\partial\phi/\partial n \simeq 0$ across the entire EDL, which is approximately valid due to the small EDL thickness and the no-penetration boundary condition of the externally applied electric field on the surfaces. This enables us to separate the volume integral in eq 29 into the following two components

$$\vec{F}_{\text{B}} = \epsilon\left[\int_0^{2h} \frac{\text{d}^2\psi}{\text{d}n^2}\,\text{d}n\right]\int_0^W\int_0^L\left[\frac{\partial \phi}{\partial l}\vec{e}_{\text{l}} + \frac{\partial \phi}{\partial s}\vec{e}_{\text{s}}\right]\text{d}l\ \text{d}s \qquad (30)$$

where L and W are the streamwise and spanwise length of the domain, respectively. Also, for a general geometry, we assumed the separation distance between the two surfaces to be $2h$. The second integral in the above equation can be obtained in the postprocessing stage, by solving the electrostatic problem. Numerical solution for the first integral requires resolution of the EDL region, which requires enhanced near-wall resolution and results in the numerical stiffness. However, this integral can be evaluated analytically in the following form:

$$\int_0^{2h} \frac{\text{d}^2\psi}{\text{d}n^2}\,\text{d}n = \int_0^{2h} \text{d}\frac{\text{d}\psi}{\text{d}n} = \frac{\zeta}{h}\left[\frac{\text{d}\psi^*}{\text{d}\eta}\right]_{-1}^{1} = 2\frac{\zeta}{h}\sqrt{\frac{\beta}{\alpha}}\sqrt{2\cosh(\alpha) - 2} \qquad (31)$$

Hence, the entire drag force can be evaluated as

$$2\epsilon\frac{\zeta}{h}\sqrt{\frac{\beta}{\alpha}}\sqrt{2\cosh(\alpha) - 2}\int_0^W\int_0^L\left[\frac{\partial \phi}{\partial l}\vec{e}_{\text{l}} + \frac{\partial \phi}{\partial s}\vec{e}_{\text{s}}\right]\text{d}l\ \text{d}s \qquad (32)$$

Finally, our approach is acceptable, since the velocity profiles are approximated reasonably well using the slip condition. Since the EDL and corresponding electroosmotic body forces are not resolved in solution of the momentum equation, the numerical stiffness of the problem is reduced. The pressure drop in the system is imposed by either the inlet and outlet pressure conditions or the specified flow rate. The drag force due to the electrokinetic effects can be calculated in the *postprocessing stage*, under the approximation of decoupling the directions of the electroosmotic and externally applied electric field potentials. This approach is valid for $\lambda/h \ll 1$ and $\lambda/R \ll 1$.

CONCLUSIONS

Motivated by the development of microscale fluid handling mechanisms with nonmoving components, we analyzed mixed

(29) Beskok, A.; Karniadakis, G. E. *Microscale Thermophys. Eng.* **1999**, *3* (1), 43−77.

electroosmotic/pressure driven flows in two-dimensional straight channels, by assuming constant ζ, constant buffer concentration, and steady Newtonian flow. Our analysis have resulted in the following:

1. The electroosmotic potential distribution ψ^* is a function of the ionic energy parameter α only, when represented in terms of the near wall coordinate $\chi = \omega y'$.

2. We defined an *effective EDL thickness* (δ_{99}) as a function of the ionic energy parameter α and have shown that the effects of the EDL are mainly confined to a zone $\chi \leq \delta_{99}$.

3. We defined an *EDL vorticity thickness* (Ω_{99}) as a function of the ionic energy parameter α and have shown that the vorticity of the fluid within the EDL is confined (mostly) to a zone $\chi \leq \Omega_{99}$.

4. For $\chi \geq 2$, both the electroosmotic potential (ψ^*) and its first space derivative ($d\psi^*/d\eta$) decay exponentially with slope of -1 as a function of χ.

5. There is a *mass flow rate defect* due to the velocity distribution within the EDL. We quantified this defect as the *EDL displacement thickness* δ^*, in analogy to the boundary layer displacement thickness in fluid mechanics.

6. Analytical solutions for the mass flow rate, pressure gradient, wall shear stress, and vorticity in mixed electroosmotic/pressure driven flows are presented.

7. We have shown that utilization of the Helmholtz−Smoluchowski velocity (eq 14) as the matching condition between the bulk flow and EDL is *incomplete* for mixed electroosmotic/pressure driven flows.

8. Helmholtz−Smoluchowski velocity becomes the appropriate slip condition, if it is imposed on the wall. However, this creates a difficulty in obtaining the drag force due to the electroosmotic body forces. We have shown that the drag force can be obtained in the postprocessing stage in an arbitrary complex geometry as along as $\lambda \ll h$ and $\lambda \ll R$.

ACKNOWLEDGMENT

This work has been funded partially by the Texas Higher Education Council, Advanced Research Program (000512-0418-1999) and partially by the Dell STAR Program.

Received for review October 3, 2000. Accepted February 13, 2001.

AC001182I